Fast Calibration of Analog to Digital Converters

By
Gina M. Kelso

B.S. University of Maine, 1997

A THESIS
Submitted in Partial Fulfillment of the
Requirements for the Degree of
Master of Science
(in Electrical Engineering)

The Graduate School
University of Maine
August, 1999

Advisory Committee:

Fred H. Irons, Castle Professor of Electrical and Computer Engineering, Advisor

Donald M. Hummels, Associate Professor of Electrical and Computer Engineering

Allison I. Whitney, Lecturer in Electrical and Computer Engineering

LIBRARY RIGHTS STATEMENT

Fast Calibration of Analog to Digital Converters

By Gina M. Kelso

Thesis Advisor: Dr. Fred H. Irons

An Abstract of the Thesis Presented

in Partial Fulfillment of the Requirements for the

Degree of Master of Science

(in Electrical Engineering)

August, 1999

Currently the performance of systems such as digital receivers is limited by the resolution of analog to digital converters. Previous research has shown that the error in converters can be modeled through calibration procedures and removed from the converter through compensation [1, 3, 4, 7, 9]. Unfortunately the existing calibration procedures are extremely time consuming making them unrealistic in digital receivers which need to be calibrated while in use.

This thesis presents a new faster method of calibrating analog to digital converters (ADC) using two wideband calibration signals. The technique is first presented for estimating error dependent on output sample and input slope, then extended to also include previous output sample dependent error. The method utilizes a harmonic based non-iterative approach for estimating the ADC error. Methods for selecting two two-tone calibration signals are also discussed. Compensation results for both simulated and actual ADC models are presented.

ACKNOWLEDGMENTS

This work has been supported in part by the ARPA HBT/ADC program under a contract administered by the Office of Naval Research Grant N000149311007, and the Army Research Office Grant DAAH04-94-G-0387.

I would first like to thank Professor Fred Irons for being an incredible mentor during the work on this thesis and for being a great friend. Professor Irons continually shows me what it means to be an outstanding engineer and person. I would like to also thank Professor Don Hummels for his guidance and answering every question. Thank you Al Whitney for your encouragement and objective approach to electrical engineering. Thank you to Gene and Paula Kelso for their love and encouragement. Finally, thank you to Mark Dominic for being my biggest supporter and helping me see what will be.

TABLE OF CONTENTS

LIST OF FIGURES

CHAPTER 1

Introduction

The need for self calibrating analog to digital converters (ADCs) continues to grow in applications such as digital receiver systems. Most commercial ADCs have resolution performance limited by the architecture of the ADC. Sources of the dynamic error and methods to correct, or compensate these errors have been researched and shown to provide significant improvements in ADC performance. Unfortunately previous schemes are extremely time consuming and test environment dependent. Operator controlled or automated calibration of the ADC in operating receiver systems would require taking the ADC offline for significant lengths of time. This thesis develops a fast multi-tone calibration scheme to determine the converter error due to the output sample, input signal slope and previous output sample.

1.1 Problem Statement

Modeling of ADC error is not a new concept. Many researchers have looked at the problem of developing an error model based on the slope of the input signal and the value of the output sample [1, 3, 7, 9]. The resulting techniques have involved generating a table of error values indexed by the output sample and the slope of the input signal. The calibration method used to determine the error values involved generating numerous sinusoidal calibration signals. The signals with varying frequency and amplitude excite the converter at combinations of the output sample and the input signal slope. These efforts resulted in error models that when used for compensation improved the performance of ADCs.

The research presented in this thesis develops methods to overcome several shortcomings of previous research. Many schemes have been limited to modeling only input signal slope error [4, 7]. Other techniques were extremely test equipment intensive generating hundreds of narrow-band calibration signals requiring numerous filters [7, 9]. These calibration techniques also involved large amounts of processing time. This past research showed little opportunity for real-time calibration and compensation of ADCs.

1.2 Purpose of the Research

This thesis describes a new calibration method for finding ADC error functions. The ADC error will be determined using multi-tone calibration signals. It is shown that multi-tone calibration signals provide the information required to determine an error model for the entire first Nyquist band without having to actually generate hundreds of single-tone signals to characterize the ADC. Multi-tone calibration signals decrease the time of calibration by decreasing the number of signals that need to be generated. This not only saves generation time but decreases the number, or switching, of filters required and the data acquisition time. The time needed to retrieve sufficient state data to determine an error estimate will be reduced from 2-4 hours to less than 5 minutes.

With decreased calibration time, multi-tone calibration makes compensation of more than one type of error mechanism feasible. A good calibration signal should excite all desired states of the converter. For different error types the desired set of converter states may be different. This thesis develops multi-tone calibration signals which are selected to provide an entire set of converter states. The ability to specialize a multi-tone signal provides the possibility of designing one signal to calibrate for mulitiple different error dependencies. This thesis presents two calibration signals developed to determine an error estimate dependent on output sample, input signal slope, and previous output sample.

1.3 Thesis Organization

This thesis describes the selection of calibration signals, the process of determining an error estimate, the incorporation of multiple error types into the process and finally, compensation of the ADC.

Chapter 2 presents and explains multi-tone calibration of input signal slope dependent errors, the process of selecting a good single calibration signal, an error modeling procedure based on a classic least squares solution, and preliminary results based on slope dependent error modeling. Chapter 3 details the addition of previous sample error modeling to the methods developed in Chapter 2, while Chapter 4 presents final simulated and actual ADC results obtained from the material developed in Chapters 2 and 3. Finally, Chapter 5 summarizes and makes recommendations for future work related to the research performed for this thesis.

CHAPTER 2

Multi-Tone Calibration

The overall goal of a calibration scheme is to determine an estimate of the error dependent on output sample and input signal slope present in an ADC. The multi-tone calibration scheme replaces a more time and test equipment intensive narrow-band method with a faster multi-tone one. The new method allows the calibration of the ADC to be sped up by at least 2 orders of magnitude which will make compensation of ADCs realizable for in-line ADC applications. The multi-tone scheme will utilize existing ideas on basis function representation of the ADC error but involve only one multi-tone calibration signal.

2.1 An Overview of ADC Calibration and Compensation

Calibrating an ADC is the process of determining an error estimate. This is done by driving the ADC with a calibration signal which will excite specific states in the converter. The converter output is collected and then used as "training" data to estimate the error. A mathematical model of the error present in the calibration data is made. The error present in the calibration data must be sufficient to model the error at every possible state in the converter. For example, the first set of converter states that this thesis will focus on is input signal slope and output sample.

In previous work this was achieved by generating multiple single-tone signals with varying frequencies and amplitudes [2, 4, 7]. The calibration signals would need to excite the converter at sample values 0 through $2^n - 1$ where n is the number of converter output bits. For each single-tone signal, x_i, the derivative of the samples produce slope values which, when normalized by the sample frequency,

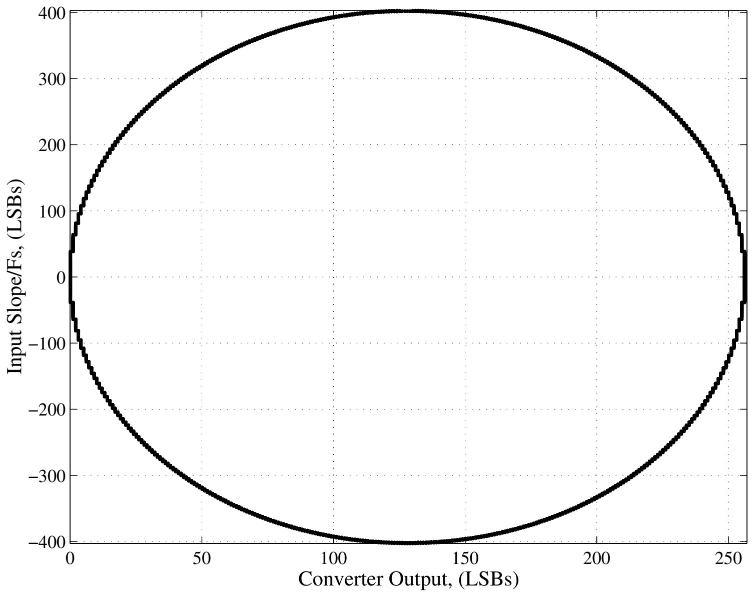

Figure 2.1: Trajectory plot for a single-tone signal in the first Nyquist band at maximum amplitude and frequency for an 8-bit converter.

f_s, gives y_i as in (2.1).

$$\begin{aligned} x_i(t) &= Acos(2\pi f_i t + \theta) \\ y_i(t) &= -\frac{A2\pi f_i}{f_s} sin(2\pi f_i t + \theta) \end{aligned} \tag{2.1}$$

A is the amplitude of the calibration signal, and f_i is the signal frequency. To obtain the maximum slope values possible in the first Nyquist band, A would be 2^{n-1} LSBs and f_i would need to be $\frac{f_s}{2}$. These selections for A and f_i result in a trajectory in the sample-slope space, or phase plane, as shown in Figure 2.1. Other single-tone calibration signals would then be selected to fill inside the maximum trajectory.

A calibration test bed setup, for calibration of an ADC using the single-tone method, is shown in Figure 2.2. The setup requires a high resolution, broadband frequency generator. The signal generator output then requires a filter bed with

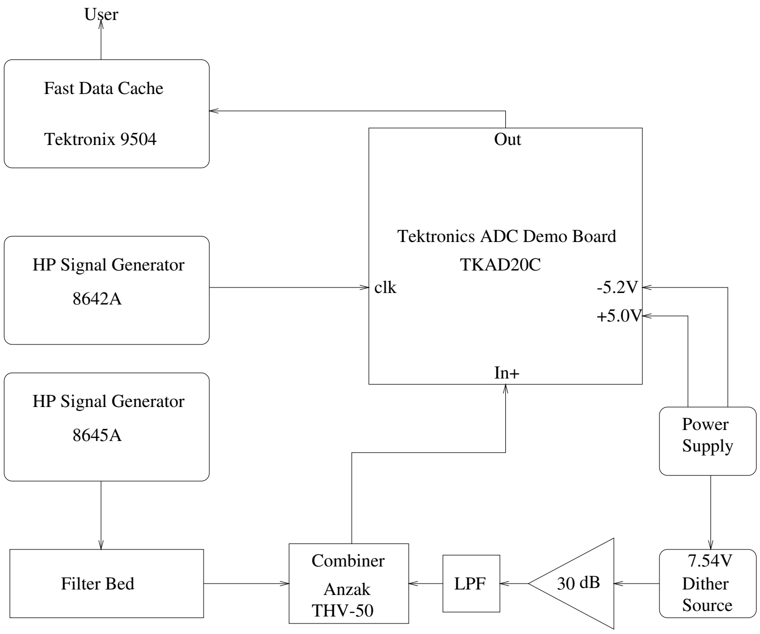

Figure 2.2: Test bed setup for single-tone calibration.

the capability to switch between as many as 10 different filters. It is clear to see why generating and filtering as many as 100 calibration signals is time consuming. For the fast multi-tone calibration, fixed frequency oscillators or high resolution digital-to-analog converters would replace the signal generator in Figure 2.2. One fixed filter would replace the need for the switched filter bank. These improvements will decrease calibration time.

Once the calibration procedure is complete, compensation of the converter can be performed. Compensation involves using the model developed in calibration to find an error value for a particular converter state. The error value is then subtracted from the converter output to provide a compensated signal. The compensation results are the measure of how well the calibration procedure estimated the error. If the compensation results do not show resolution improvement across the entire frequency band of interest, then the calibration signal or mathematical model may need to be adjusted.

To speed up these existing calibration procedures a multi-tone calibration procedure will be developed. The phase plane will be looked at with multi-tone signals and the algorithm to determine the error estimate will be modified to acommadate multi-tone data. A successful multi-tone procedure will significantly reduce the calibration time presently needed for single-tone schemes.

2.2 Covering the Phase Plane with a Multi-Tone Signal

In order to model the ADC's dynamic error due to the input slope and output sample values, the calibration data must be collected. For purposes of this work, ADC samples are collected and estimates made of the input slope. The training, or calibration data from the multi-tone signal must excite as many of the states in the sample-slope space, or phase plane as possible. A visual representation of the signal's ability to excite these combinations is shown in the phase plane. The plane is created by plotting output sample values against estimates of the input slope. An ideal calibration signal fills the phase plane evenly out to the full scale limits of the ADC. Therefore, an ideal calibration signal provides sufficient data at all possible combinations of sample and slope.

In previous research sufficient data for calibration was collected by acquiring numerous single-tone calibration signals each at varying frequencies and amplitudes. An example of the resulting maximum elliptical trajectory in the sample slope space is shown in Figure 2.1. To fill the space inside of this trajectory, the converter is driven by 50-100 calibration signals using varying amplitude, A, and frequencies, f_i. This process is not only time intensive, but requires a high resolution signal source and filtering. To eliminate the process of generating multiple calibration signals and collecting the resulting ADC output for each calibration signal, the feasibility of filling the space inside the maximum trajectory shown in Figure 2.1 is investigated. When it is possible to select a single signal to cover the sample-slope space, then calibration can be done with only one signal.

In order for multi-tone signal calibration to be successful, the calibration signal must provide data along and inside the maximum trajectory discussed in Section 2.1. The input signal and slope for the multi-tone signal can be found as a sum of m single-tone signals x_i found in (2.1).

$$x_m(t) = \sum_{l=1}^{m} A_l cos(2\pi f_l t + \theta_l) \tag{2.2}$$

$$y_m(t) = \sum_{l=1}^{m} -\frac{A_l 2\pi f_l}{f_s} sin(2\pi f_l t + \theta_l) \tag{2.3}$$

Therefore, to maximize the output sample values and input slope values, the values for A_l and f_l will need to be carefully selected. From the single-tone signal case, it is known that a maximum amplitude of $2^{n-1} LSBs$ and a maximum tone frequency of $\frac{f_s}{2}$ are necessary. From (2.2), the maximum case would give the condition (2.4).

$$\max(x_m(t)) \leq \sum_{l=1}^{m} A_l \leq 2^{n-1} \tag{2.4}$$

For m equal amplitudes, A_l is required to be

$$A_l \leq \frac{2^{n-1}}{m} \tag{2.5}$$

The maximum slope values from (2.3) can be determined as follows.

$$\max(y_m(t)) \leq \sum_{l=1}^{m} \frac{A_l 2\pi f_l}{fs}$$

Given the upperbound given by (2.5), the maximum slope would occur when the average value of f_l is near but less than the Nyquist frequency.

$$\max(y_m(t)) \leq \frac{2\pi 2^{n-1}}{fs} \frac{1}{m} \sum_{l=1}^{m} f_l \tag{2.6}$$

If

$$\frac{1}{m}\sum_{l=1}^{m} f_l \leq \frac{fs}{2} \tag{2.7}$$

then

$$\max(y_m(t)) \leq \pi 2^{n-1} \tag{2.8}$$

Selecting A_l as in (2.5) and f_l as in (2.7), gives data points along the maximum trajectory. For input signals within the first Nyquist band ($0 < f_l < \frac{f_s}{2}$), this implies that all m signals must be close to $\frac{f_s}{2}$, resulting in a narrow-band calibration signal. Now a selection for m must be made.

Examination of a five-tone signal was performed first. The five tones, each with equal amounts of energy, are placed near Nyquist. The selected frequencies will drive the ADC over the maximum possible input slope values, while keeping equal energy in all tones prevents a void of data in the middle of the sample-slope space. Figure 2.3 shows the resulting sample-slope space plot for an 8-bit converter. The different combinations of input slope and output samples tend to concentrate in the center (i.e.- become Gaussian distributions). Careful examination of the sample slope space for the five-tone signal shows a lack of data points near the maximum and minimum of the possible sample and slope values. As an alternative to the five-tone signal, a two-tone signal was also examined.

The two-tone signal was selected to have equal energy in both tones and with the frequency of the tones just below the Nyquist frequency. The resulting trajectory in the signal space is shown in Fig. 2.4. Experimentation shows that the two-tone signal has a more uniform distribution of data combinations over the space than the five-tone signal. A two-tone signal provides better coverage and will be used to perform the multi-tone calibration.

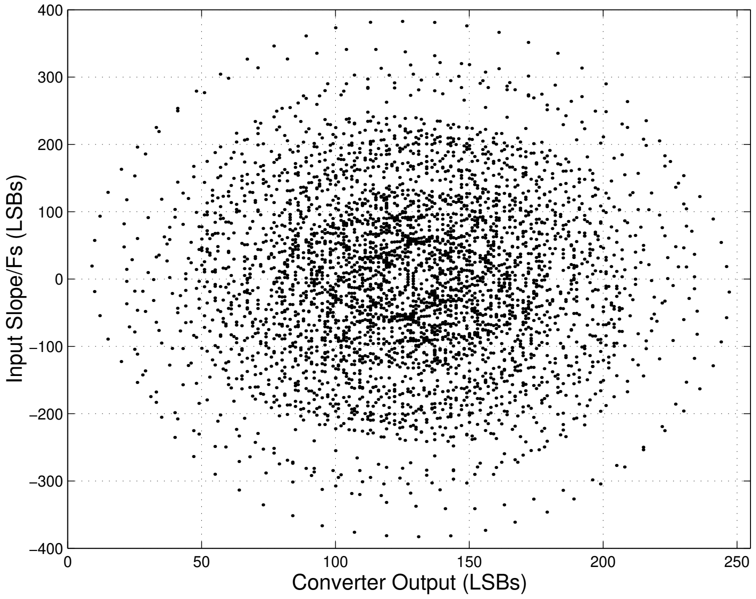

Figure 2.3: Trajectory plot for a five-tone signal.

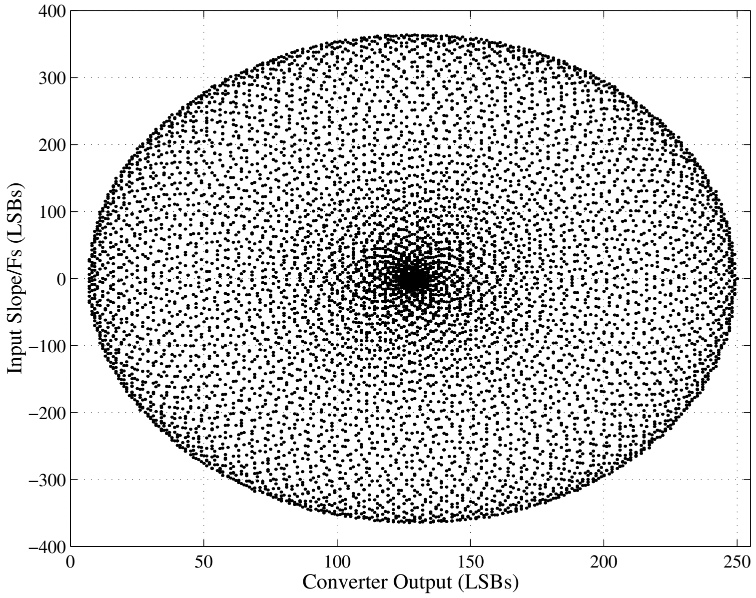

Figure 2.4: Trajectory plot for a two tone signal.

2.3 Selecting the Multi-Tone Calibration Signal

The two-tone signal was selected for calibration over the five-tone signal. To select the calibration signal there are three qualities to consider for each tone: amplitude (both relative and absolute), frequency, and phase. To completely understand how these affect the phase plane, the parameters are examined separately.

The amplitude of each tone is important as well as the difference in amplitude between the tones. To maintain the coverage shown in Figure 2.4, the amount of energy in each tone should be the same. If the amplitude of one tone is larger, a "hole" or void of states will appear in the middle of the phase plane. Also if the overall energy in both tones is not close to the full scale of the converter input, the phase plane will not be filled. This can be seen in the phase plane of an 8-bit ADC shown in Figure 2.5. The signal amplitude is limited to 75% of the converter's full scale. Then one of the tones was dropped 1.5 dB below the other. Not only did the space shrink but states near zero slope and converter output 128 LSBs are not excited.

The frequencies of the tones were carefully selected. The tone frequencies, f_1 and f_2 were found by selecting FFT bins m_1 and m_2 as shown in (2.9).

$$
\begin{aligned}
f_1 &= m_1 * f_s/N \\
f_2 &= m_2 * f_s/N
\end{aligned}
\tag{2.9}
$$

m_1 and m_2 were first selected to place the tones near the Nyquist frequency $f_s/2$. This produces many of the higher slope values necessary to cover the space. Poor selections of m_1 and m_2 can create a defined repeating pattern in the data combinations. These undesirable patterns, where a large majority the points take on the same value, occur when the greatest common divisor between m_1 and m_2 is not 1. An example of this is shown in Figure 2.6. Therefore, m_1 and m_2 need

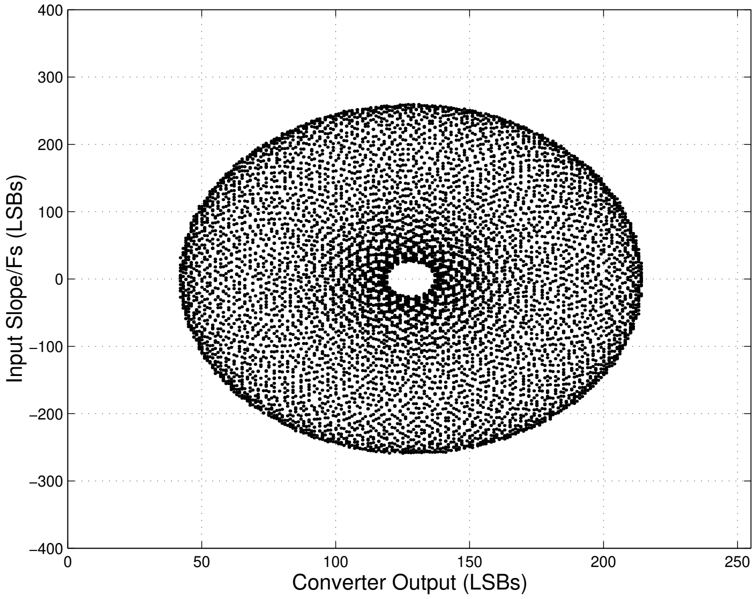

Figure 2.5: Trajectory plot for a two-tone signal with low and unequal amplitudes.

to be relatively prime. Selecting these frequencies can leave significant gaps in calibration data.

Experience has shown that the two-tone signal trajectory is not affected by the phase of the two tones used to make the signal.

Given the above considerations, the calibration signal (calibration signal 1) is limited to 90% of full scale of the ADC output. For simulation and actual ADC results, the phase was considered to be random. A buffer of 8192 samples was collected from an ADC sampled at 204.8 MSPS. The tones were placed at FFT bins 3953 and 3891. The tone frequencies were 98.825 MHz and 97.275 MHz. The sample-slope space of the chosen calibration signal is shown in Figure 2.4. A spectrum of the signal is given in Figure 2.7.

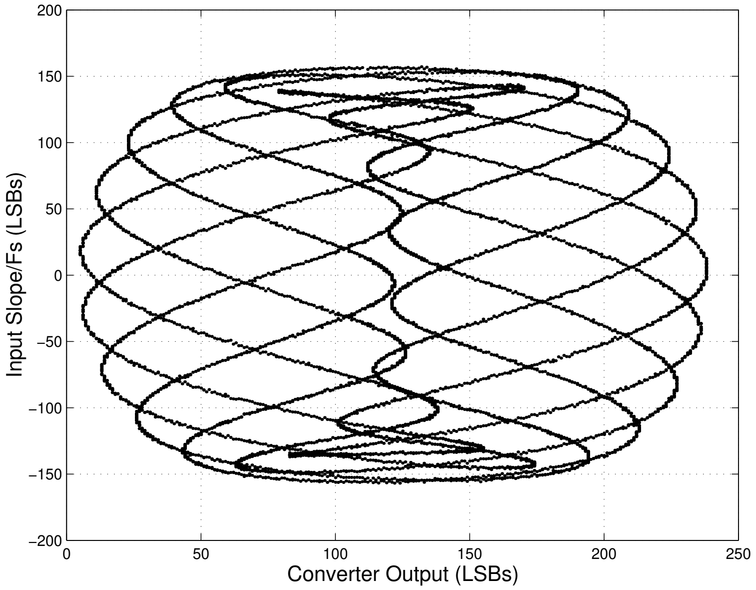

Figure 2.6: Trajectory plot for a two-tone signal with poor selections for m_1 and m_2.

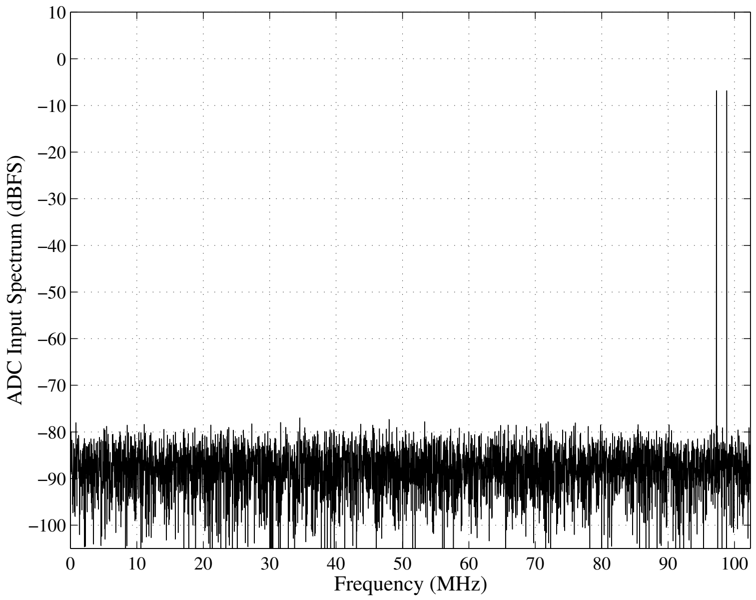

Figure 2.7: Spectrum of the two-tone calibration signal.

2.4 Two-Tone Calibration

A two-tone signal was selected to calibrate the ADC. The calibration procedure develops an estimated error value dependent upon the sample and slope values. To determine the error estimates, the error is written using a basis function representation where the coefficients of the basis functions are determined using least-squares approximation techniques.

2.4.1 Multi-tone Calibration Procedure

Error correction is performed by creating a lookup function, or table, of error values. The error values are assumed to be a function of the ADC output code, x, and the slope of the input signal, y. Let $e(x, y)$ denote the error introduced by the ADC. If $e(x, y)$ is known, then the ADC output may be compensated to remove distortion as shown in (2.10).

$$x_c = x - e(x, y) \tag{2.10}$$

The goal of calibration is to create an error function $e(x, y)$ to produce a distortion free sample, x_c.

During calibration, the ADC is driven with a two-tone signal as shown in Figure 2.7. An N-sample buffer of ADC outputs is collected and used to form the vector $\vec{x}$, of output samples. The input slopes, $\vec{y}$, were estimated from the derivative of $\vec{x}$.

To estimate the error functions, a basis-function representation of $e(x, y)$ is adopted.

$$e(x, y) = \sum_{i=1}^{L} \alpha_i b_i(x, y) \tag{2.11}$$

In (2.11), $b_i(x, y)$ are known basis functions. The calibration process involves the selection of appropriate values for the coefficients, α_i, to minimize the residual distortion in x_c of (2.10). Evaluating (2.11) at the calibration data gives a vector form of (2.11) for the measured sample set:

$$\begin{aligned} \vec{e}(\vec{x}, \vec{y}) &= \sum_{i=1}^{L} \alpha_i \vec{b}_i(\vec{x}, \vec{y}) && (2.12) \\ &= B\vec{\alpha} && (2.13) \end{aligned}$$

where

$$\begin{aligned} \vec{b}_i(\vec{x}, \vec{y}) &= [b_i(x_1, y_1) \;\; b_i(x_2, y_2) \;\; \ldots \;\; b_i(x_N, y_N)]^T && (2.14) \\ B &= [\vec{b}_1(\vec{x}, \vec{y}) \;\; \ldots \;\; \vec{b}_L(\vec{x}, \vec{y})] && (2.15) \\ \vec{\alpha} &= [\alpha_1 \;\; \alpha_2 \;\; \ldots \;\; \alpha_L]^T && (2.16) \end{aligned}$$

The compensated calibration signal, x_c, is obtained by subtracting the error function from the calibration buffer

$$\vec{x}_c = \vec{x} - B\vec{\alpha} \qquad (2.17)$$

For the given calibration signal, a set of possible distortion frequencies $f_1, f_2, ...f_M$ are identified based on low-order intermodulation components and harmonics of the input signal frequencies. The unknown coefficients $\vec{\alpha}$ are determined by minimizing the distortion at these frequencies in the compensated signal, $\vec{x}_c$, of (2.17).

FFT coefficients, at the M selected distortion frequencies, are obtained by multiplying (2.17) by a transform matrix T given by (2.18)

$$T = \begin{bmatrix} W_1^0 & W_1^1 & W_1^2 & W_1^3 & \dots & W_1^{N-1} \\ W_2^0 & W_2^1 & W_2^2 & W_2^3 & \dots & W_2^{N-1} \\ W_3^0 & W_3^1 & W_3^2 & W_3^3 & \dots & W_3^{N-1} \\ & \vdots & & & & \\ W_M^0 & W_M^1 & W_M^2 & W_M^3 & \dots & W_M^{N-1} \end{bmatrix} \tag{2.18}$$

where

$$W_k = e^{-j2\pi\frac{k}{N}}$$

and

$$\frac{k}{N} = \frac{f_k}{f_s}$$

This process gives

$$\vec{x}_{T_c} = \vec{x}_T - B_T\vec{\alpha} \tag{2.19}$$

where

$$\vec{x}_{T_c} = \begin{bmatrix} Re(T\vec{x}_c) \\ Im(T\vec{x}_c) \end{bmatrix}$$

$$\vec{x}_T = \begin{bmatrix} Re(T\vec{x}) \\ Im(T\vec{x}) \end{bmatrix}$$

$$B_T = \begin{bmatrix} Re(TB) \\ Im(TB) \end{bmatrix} \tag{2.20}$$

A least-squares procedure yields $\vec{\alpha}$ so as to minimize the distortion power in $T\vec{x}_c$

at the M selected frequencies.

In implementation, the i^{th} column of TB is found by using the FFT of $\vec{b}_i(\vec{x}, \vec{y})$, and selecting appropriate harmonics. Similarly the elements for $T\vec{x}$ are found by performing an FFT on $\vec{x}$. Finding an approximation of α in a least squares sense leads to (2.21).

$$((B_T)^T(B_T))\hat{\vec{\alpha}} = (B_T)^T(\vec{x}_T) \tag{2.21}$$

If the Gram matrix $((B_T)^T B_T)$ is nonsingular, the solution is given by (2.22).

$$\hat{\vec{\alpha}} = ((B_T)^T(B_T))^{-1}(B_T)^T(\vec{x}_T) \tag{2.22}$$

Since the inverse of the Gram matrix caused instability in the estimation of α, a singular-value decomposition technique was used to solve (2.21). The technique of using the singular-value decomposition of $(B_T^T B_T)$ to find $\hat{\alpha}$ is described in the Appendix.

From the calibration procedure an estimate of α is determined based on predetermined basis functions. The functions and coefficients are then be used to compensate the ADC output using (2.10) and (2.11).

2.5 Multi-tone Calibration and Compensation Results Based on Output Sample and Input Slope Dependent Error

Now that a calibration signal and procedure has been established, testing of the technique needs to be done. The procedure will first be simulated to test the validity of the algorithm, and then tested on an actual ADC to establish calibration performance. The effectiveness of the calibration can be measured by compensating the samples, $\vec{x}$, of single-tone signals. The estimated error value,

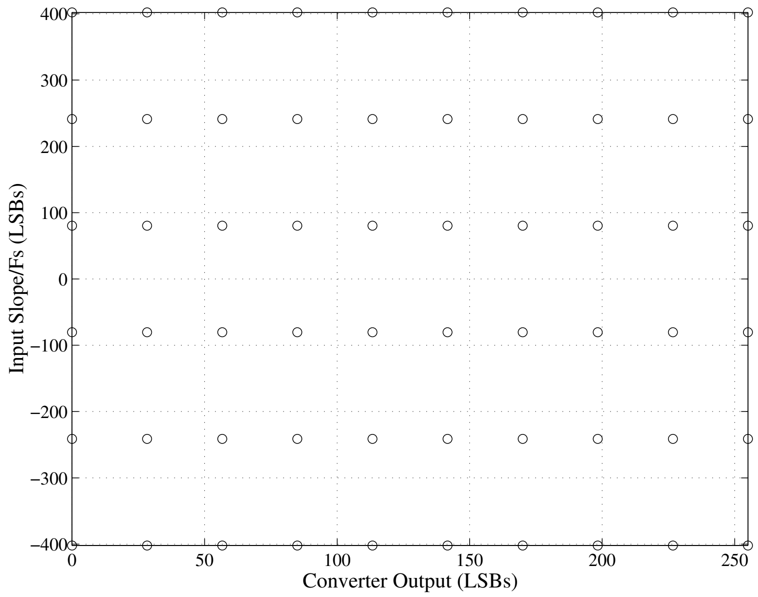

Figure 2.8: (c_{x_i}, c_{y_i}) basis function centers for $i = 1, \ldots, 60$.

$e(x, y)$, is then subtracted from the sample, x, to provide a compensated sample, x_c.

2.5.1 ADC Simulation Results

The concepts developed in the previous sections were tested on a model of an 8-bit converter sampled at 204.8 MHz. The converter model was based on a flash ADC architecture and contained only slope-dependent error. The algorithm used Gaussian basis functions given in (2.23) with the basis function centers distributed on a 10×6 grid. Figure 2.8 shows the centers of the basis functions, c_{x_i} and c_{y_i} in the phase plane for an 8-bit converter. The standard deviation for each basis function was set to be equal to the separation of the function's centers on each axis. For the sample axis the standard deviation, σ_x was 28.34 and for the slope axis, σ_y was 160.85.

$$b_i(x, y) = e^{-\frac{1}{2}\left[\left(\frac{x - c_{x_i}}{\sigma_x}\right)^2 + \left(\frac{y - c_{y_i}}{\sigma_y}\right)^2\right]} \tag{2.23}$$

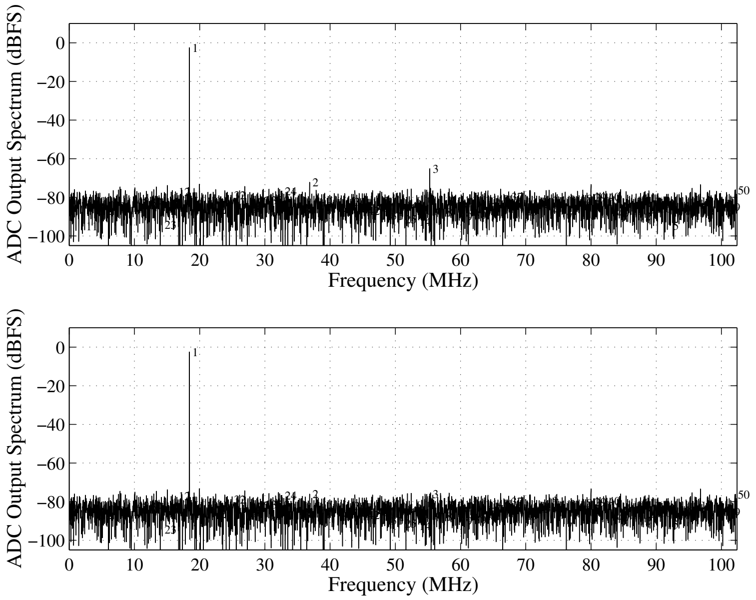

Figure 2.9: Uncompensated and compensated magnitude spectra, simulated results for a low frequency.

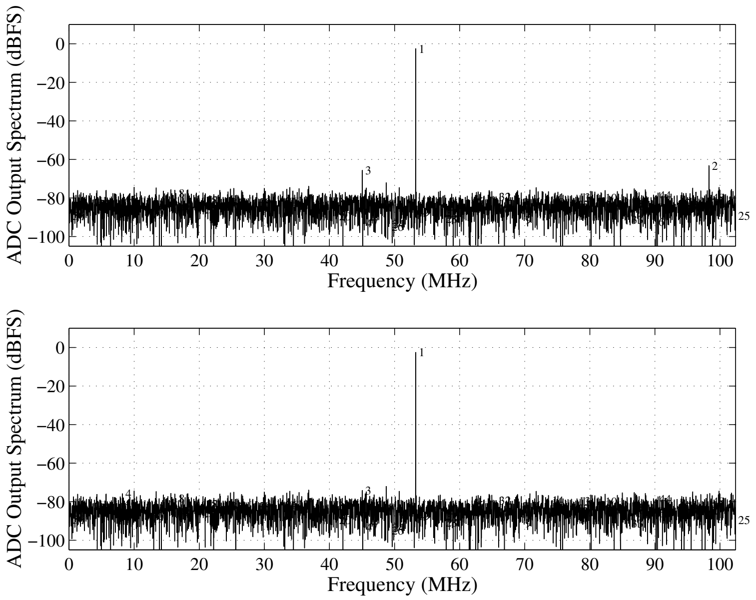

Figure 2.10: Uncompensated and compensated magnitude spectra, simulated results for a mid-Nyquist frequency.

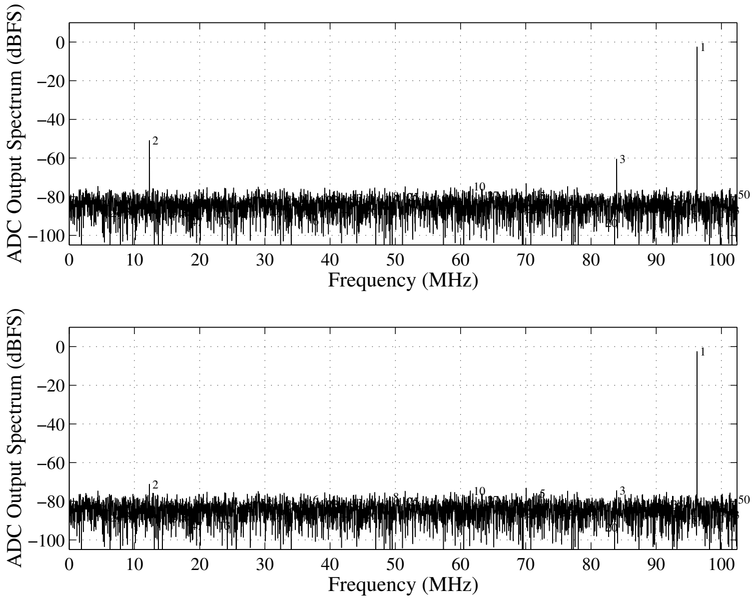

Figure 2.11: Uncompensated and compensated magnitude spectra, simulated results for a near-Nyquist frequency.

Figures 2.9 through 2.11 show uncompensated and compensated magnitude spectra for the simulated model. These results were based on using 12^{th} order intermodulation terms to determine the converter error. In (2.18), N would be equal to 12. The plots show results for testing low, mid and near-Nyquist frequencies. These results clearly show the single two-tone calibration signals ability to model slope dependent errors at different sections of the first Nyquist band.

The performance of the simulated multi-tone calibration scheme can also be seen in Figure 2.12. The plot shows the spurious-free dynamic range (SFDR) for the simulated converter before and after compensation. The simulated converter was driven by a single-tone signal and the difference between the height of the fundamental and the next highest spurious signal is taken to be the SFDR. The results show SFDR improvements over the entire first Nyquist band of the ADC. The simulation demonstrates the algorithm's potential to estimate wideband sample and slope dependent error.

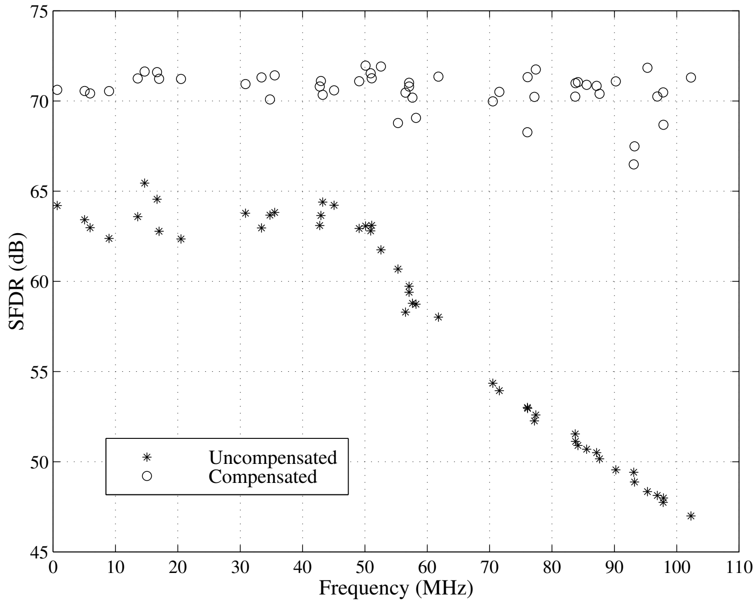

Figure 2.12: SFDR plot, simulated results.

2.5.2 ADC Experimental Results

This section presents experimental data obtained from an 8-bit ADC. The ADC is clocked at 204.8 MHz and one 16K buffer of output data is collected. The two-tone calibration signal used had equal energy at 98.825 MHz and 97.275 MHz. The magnitude spectrum of this signal is shown in Figure 2.7. Figures 2.13 through 2.15 show uncompensated and compensated magnitude spectra for the experimental ADC. Figure 2.13 shows little to no improvement in SFDR measure. Mid-band testing in Figure 2.14 again shows little improvement in SFDR; in fact, the 3^{rd} harmonic is larger after compensation. Some improvement in SFDR can be seen in Figure 2.15. To fully grasp what is happening across the entire first Nyquist band SFDR measurements were gathered for signals placed across the band. The results are shown in Figure 2.16. The calibration scheme appears to only be estimating slope errors at frequencies near Nyquist where slope dependent errors might be expected to dominate. This area also coincides with the frequencies

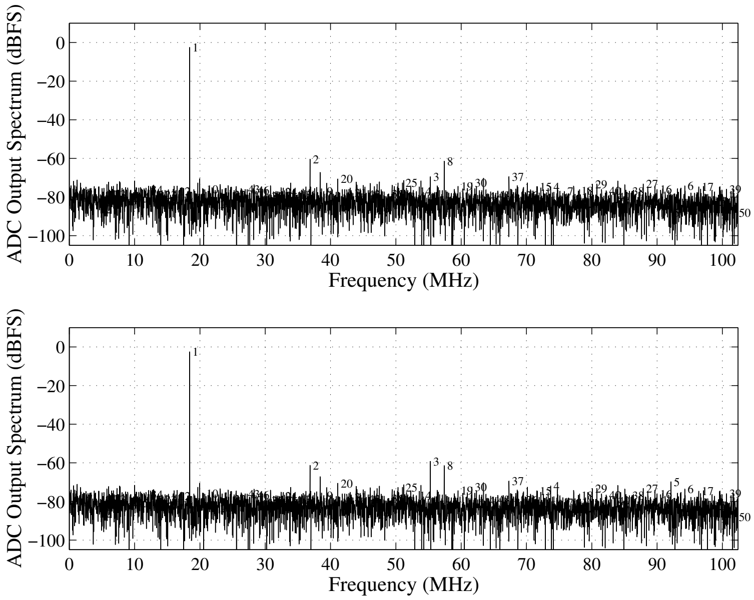

Figure 2.13: Uncompensated and compensated magnitude spectra, experimental results for a low frequency.

used for calibration.

2.6 Summary of Slope Dependent Error Calibration

One of the primary goals of the multi-tone calibration scheme signal is to provide improvement in SFDR at frequencies across the entire Nyquist band. From initial examination of the SFDR experimental results, it appears that the multi-tone calibration routine is unable to estimate slope dependent errors in the lower two thirds of the first Nyquist band. Rigorous attempts were made to make the simulation algorithm fail in a similar manner. Numerous complex ADC models involving slope dependent error were simulated to test the algorithm. Still the simulation algorithm showed wideband compensation of the slope dependent error. In an attempt to determine why the algorithm failed on the experimental ADC, other sources of harmonic distortion were considered.

When looking at harmonic based error in the ADC, it was assumed that

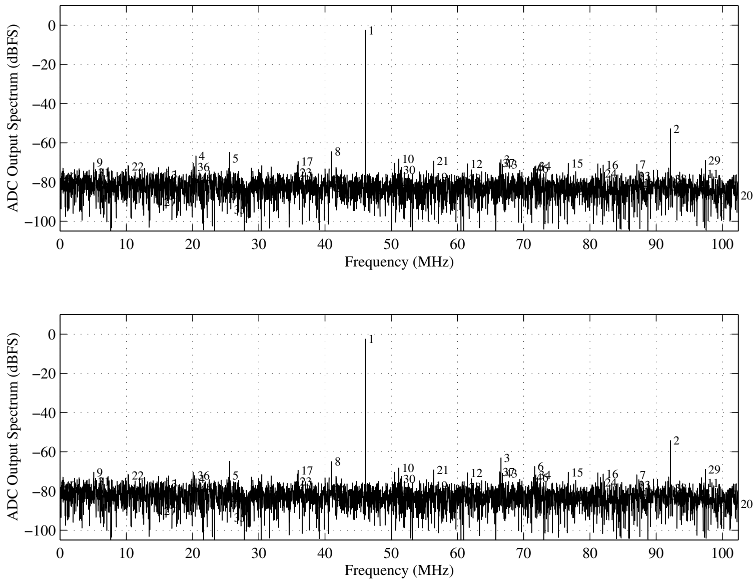

Figure 2.14: Uncompensated and compensated magnitude spectra, experimental results for a mid-Nyquist frequency.

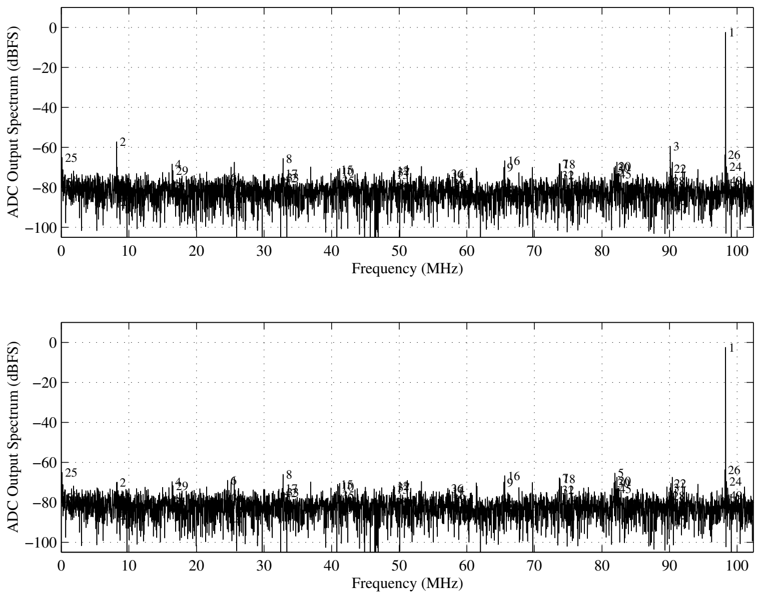

Figure 2.15: Uncompensated and compensated magnitude spectra, experimental results for a near-Nyquist frequency.

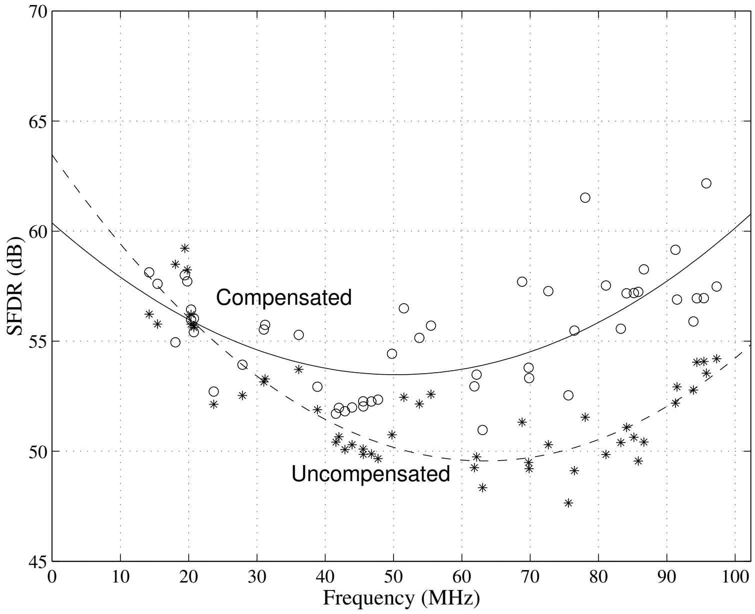

Figure 2.16: SFDR response, experimental results.

the dominant error source across the first Nyquist band was a function of the sample value and input slope only. Another possible source of harmonic distortion in ADCs is error based on the previous sample [2, 10]. The experimental results suggest the the presence of another error source. A more accurate model for the experimental ADC, which includes error due to previous samples, was used in the simulation algorithm. The SFDR measurements for these simulations prove to be similar to those taken from the experimental ADC. These results are shown in Figure 2.17. This result is important because the simulations fail in a fashion similar to the experimental result. The next chapter continues the development of the multi-tone calibration scheme by modifying the algorithm given in this chapter to incorporate the error dependence on the previous ADC output sample.

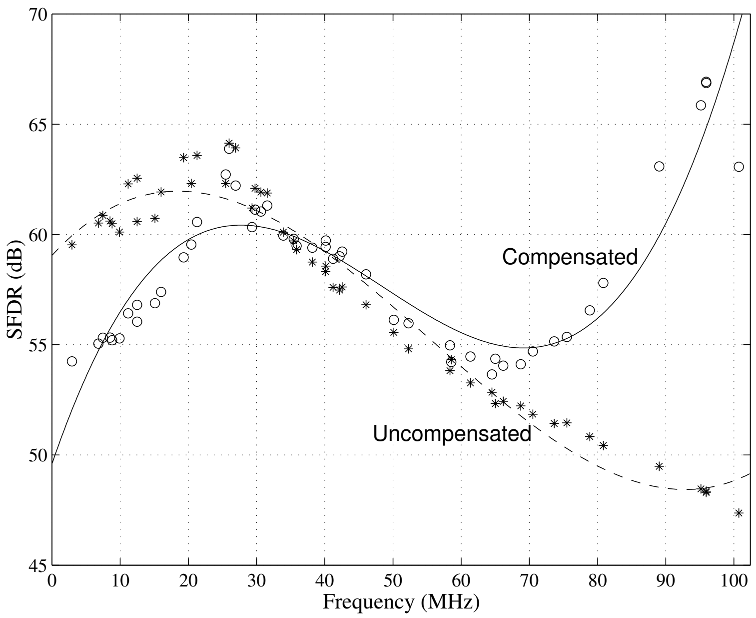

Figure 2.17: SFDR plot, simulation results.

CHAPTER 3

Multi-tone Calibration of Sample, Slope and Previous Sample Dependent Error

Chapter 2 developed a wideband calibration signal process for determining an error model dependent only on the slope of the input signal. Experimental testing of the algorithm on the actual ADC showed that there was slope dependent error present in the ADC at higher frequencies in the Nyquist band. The experimentation also suggested that another source of distortion is present in the converter. This chapter extends the wideband calibration process to include error dependency on the previous output sample as well as the slope of the input signal. To develop the final calibration algorithm, both the sample-previous sample space and the sample-input signal slope space need to be filled by the calibration signals.

3.1 Covering the Sample-Previous Sample Space

The signal shown in Figure 2.7 was selected in the previous chapter to cover the output sample-input slope space. To cover the sample-previous sample space, one would prefer to use this signal avoiding the requirement to obtain additional calibration data. Figure 3.1 depicts the first calibration signal, or calibration signal 1, in both the sample-slope space and in the sample-previous sample space. It is clear that the first calibration signal excites only a very small portion of all possible combinations of sample and previous sample values. In order to excite more combinations in the sample-previous sample space, the frequencies of the two tones in the calibration signal need to be adjusted. Doing this improves the number of different combinations of current sample and previous sample to determine an error model. Unfortunately, changing the calibration signal frequencies can decrease

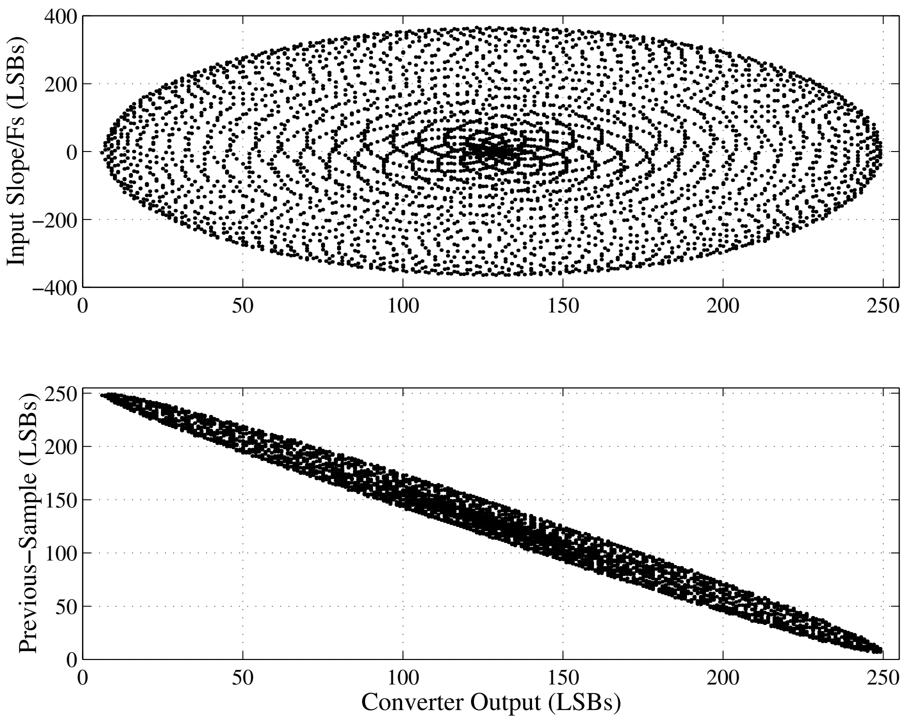

Figure 3.1: Calibration signal 1 trajectory plots.

the coverage obtained in the input slope space and reduce the integrity of slope dependent error estimates. The loss of overall compensation performance would out-weigh the gained speed of using only one calibration signal. Therefore a second multi-tone calibration signal needs to be generated.

Multi-tone signals have been shown to cover the entire sample-previous sample space [2, 5]. For this thesis, hardware limitations forced the consideration of two-tone signals only. To select this two-tone signal, one tone is placed in the lower third of the first Nyquist band and the second tone placed slightly above the middle of the band. This spreads the data points out across the possible space. The phase of the tones does not effect the signal trajectory. The spectral plot of the second calibration signal or calibration signal 2, is shown in Figure 3.2. The sampling frequency of the 8-bit ADC is 204.8 MSPS. The tones were placed at FFT bins 1105 and 2151. The tone frequencies were 27.760 MHz and 53.722 MHz.

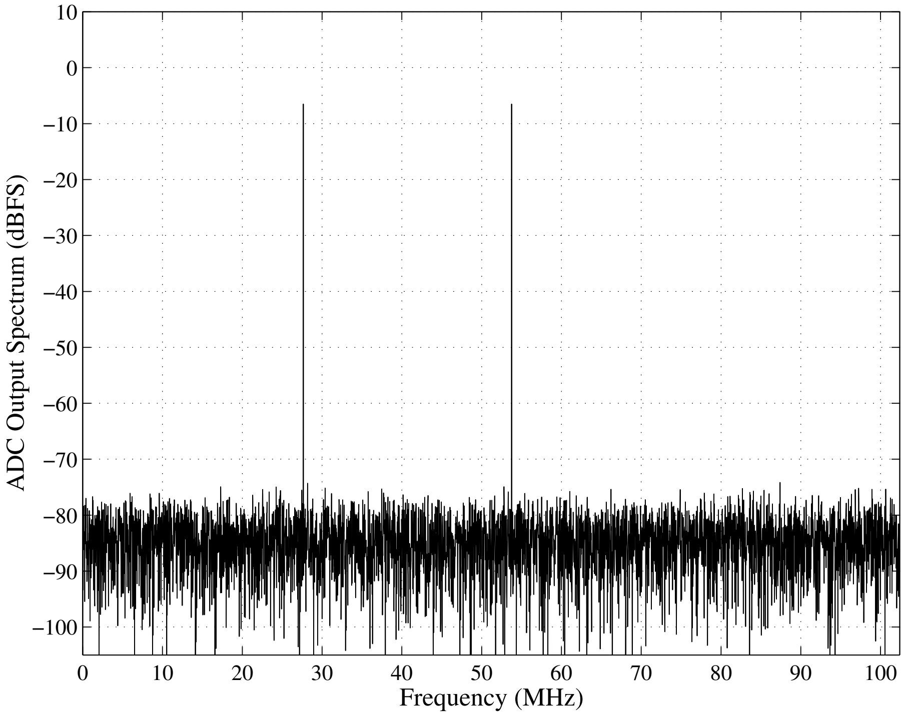

Figure 3.2: Spectrum of the second two-tone calibration signal.

Each tone does contain approximately the same amount of energy to prevent a void in the center of the combination cluster.

The sample-slope space and the sample-previous sample space for the second calibration signal is shown in Figure 3.3. In the input signal slope space, calibration signal 2 does not contribute any significant combinations of sample and slope for estimating error dependent on the input slope. In the previous sample space the signal covers a large portion of the possible combinations of current and previous output samples. Finally, to observe how well the two calibration signals cover the sample-slope space and the sample-previous sample space, the calibration signals are plotted together in Figure 3.4. The calibration signals provide thorough coverage in the sample-slope space. In the current sample-previous sample space the two calibration signals do not provide complete coverage of all possible combinations of current sample and previous sample. The coverage of the

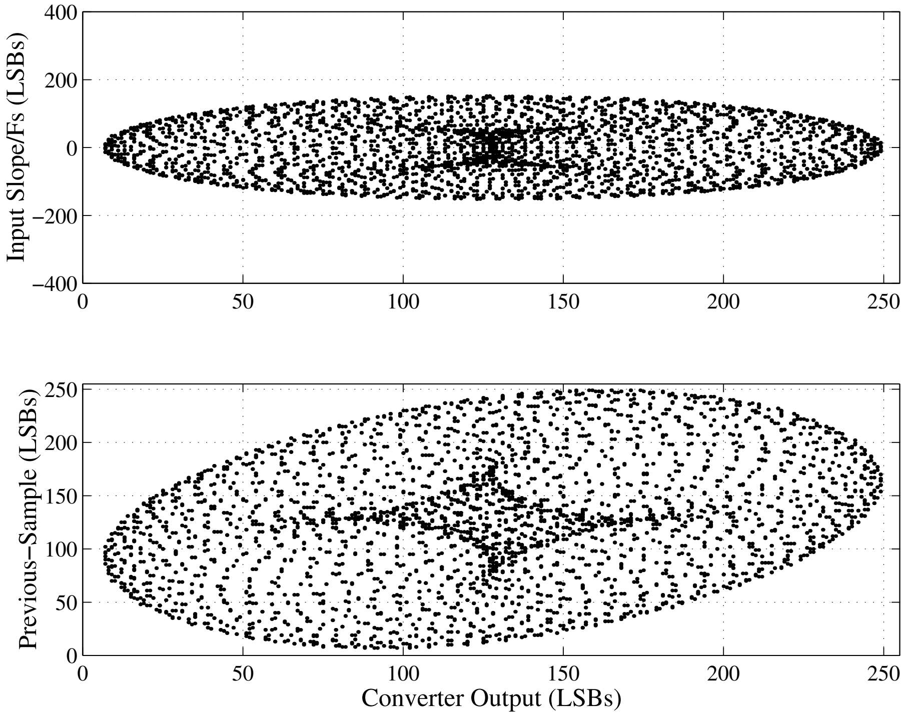

Figure 3.3: Calibration signal 2 trajectory plots.

sample-previous sample space is limited by the use of two-tone signals. The gaps in coverage shown in Figure 3.4 will have to be taken into account when examining the simulation and experimental results of the modified calibration routine.

3.2 Modified Calibration Procedure

The calibration procedure developed in Section 2.4.1 yielded an algorithm to find error estimates dependent upon variables x, the ADC output code, and y, the slope of the input signal. In this section the procedure is modified to accomodate an additional variable z, the previous ADC output code. The error function then becomes $e(x, y, z)$. Therefore the distortion free sample x_c is as follows.

$$x_c = x - e(x, y, z) \tag{3.1}$$

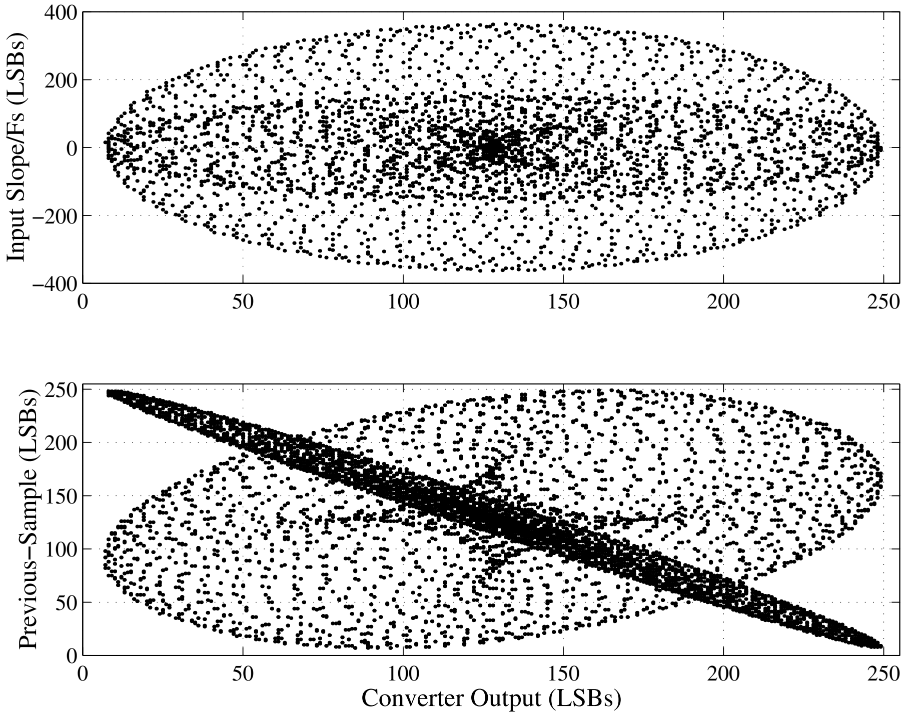

Figure 3.4: Calibration signals 1 and 2 trajectory plots.

This thesis assumes that the distortion due to the slope and the distorion due to the previous sample are uncoupled. This is a valid assumption if the sources of the error in the converter are considered. The slope dependent error is due to input amplifier compression and slew effects. The previous sample dependent error is related to track and hold errors at the input to the flash comparator array. The uncoupling of these error sources produces a more restrictive form for $e(x, y, z)$.

$$e(x, y, z) = e_1(x, y, 0) + e_2(x, 0, z) \tag{3.2}$$

With this assumption, the basis-function representation of (3.2) is rewritten.

$$e(x, y, z) = \sum_{i=1}^{K} \alpha_i b_i(x, y, 0) + \sum_{i=K+1}^{L} \alpha_i b_i(x, 0, z) \tag{3.3}$$

An N-sample buffer of ADC outputs is collected and forms the vectors, $\vec{x}$, of N output samples, $\vec{y}$, of the associated input-slope approximations, and $\vec{z}$, of N previous output samples for each calibration signal. The additional calibration variable, z, alters the measured buffer equation as follows.

$$\vec{e}(\vec{x},\vec{y},\vec{z}) = \sum_{i=1}^{K} \alpha_i \vec{b}_i(\vec{x},\vec{y},\vec{0}) + \sum_{i=K+1}^{L} \alpha_i \vec{b}_i(\vec{x},\vec{0},\vec{z}) \tag{3.4}$$

So for each calibration signal we get (3.7).

$$\begin{aligned} \vec{e}(\vec{x},\vec{y},\vec{z}) &= B\vec{\alpha} && (3.5)\\ B &= [\vec{b}_1(\vec{x},\vec{y},\vec{0}) \ \ldots \ \vec{b}_K(\vec{x},\vec{y},\vec{0}), \vec{b}_{K+1}(\vec{x},\vec{0},\vec{z}) \ \ldots \ \vec{b}_L(\vec{x},\vec{0},\vec{z})] && (3.6)\\ \vec{\alpha} &= [\alpha_1 \ \ \alpha_2 \ \ \ldots \ \ \alpha_L]^T && (3.7) \end{aligned}$$

As in section 2.4.1 a least squares approximation to $\vec{\alpha}$ can be found by solving (3.8).

$$((B_T)^T(B_T))\hat{\vec{\alpha}} = (B_T)^T(\vec{x}_T) \tag{3.8}$$

Let $(\vec{x_1},\vec{y_1},\vec{z_1})$ be the ADC output samples, the input slope and the previous sample taken when the converter is driven by calibration signal 1. Let B_1 be the matrix formed in (3.6) evaluated from calibration signal 1 data $(\vec{x_1},\vec{y_1},\vec{z_1})$. Similarly let $(\vec{x_2},\vec{y_2},\vec{z_2})$ be the ADC output samples, the input slope and the previous sample taken when the converter is driven by calibration signal 2, and let B_2 be the matrix formed in (3.6) evaluated from calibration signal 2 data. For the multisignal calibration B_T and $\vec{x}_T$ are as follows.

$$B_T = \begin{bmatrix} Re(TB_1) \\ Im(TB_1) \\ Re(TB_2) \\ Im(TB_2) \end{bmatrix} \quad \text{and} \qquad \vec{x}_T = \begin{bmatrix} Re(\vec{x}_{T_1}) \\ Im(\vec{x}_{T_1}) \\ Re(\vec{x}_{T_2}) \\ Im(\vec{x}_{T_2}) \end{bmatrix} \tag{3.9}$$

Now $\hat{\vec{\alpha}}$ can be determined from (3.8).

3.3 Calibration Algorithm Summary

The following are the necessary steps to determine the basis function coefficients for an error model dependent on both input slope and previous sample.

1. Collect a set of samples from the ADC driven by calibration signal 1.

2. Extract relevant harmonics from an FFT of samples to form $T\vec{x}_1$.

3. Form TB_1 by evaluating each basis function $b_i(\vec{x}_1, \vec{y}_1, \vec{z}_1)$ and extracting the relevant harmonics from the FFT of each basis function.

4. Collect a set of samples from the ADC driven by calibration signal 2.

5. Extract relevant harmonics from an FFT of the sample set. Concatenate these values with $T\vec{x}_1$ from step 2 to create $\vec{x}_T$ as shown in (3.9).

6. Evaluate each basis function $b_i(\vec{x}_2, \vec{y}_2, \vec{z}_2)$. Concatenate the relevant harmonics from the FFT of each b_i on to TB_1 to form B_T as shown in (3.9).

7. Solve for $\hat{\vec{\alpha}}$ from (3.8) using singular value decomposition to perform the matrix inverse.

Once the coefficients have been determined, compensation is accomplished by applying (2.17) to output sample sets.

CHAPTER 4

Results

A multi-tone calibration procedure, for determining error dependent on ADC output sample x, input slope y, and previous ADC output sample z, has been developed. The estimated error value can then be subtracted from the sample x to provide a compensated sample, x_c. This chapter presents results obtained for the compensation of both a simulated ADC and an actual ADC.

The following results were generated using basis functions for $e_1(x, y, 0)$ being Guassian functions with their centers distributed on a 10×6 grid. The basis functions for $e_2(x, 0, z)$ are also Guassian functions but their centers are distributed on a 10×10 grid. The basis function is given in (2.23). Basis function centers for the x axis begin at 0 LSB and end with the last center at the edge of the axis at $2^{N_{bits}} - 1$ LSBs. The basis function centers for the z axis are placed in the same way as those for the x axis. For the y axis the centers are also located to the edge of the maximum and minimum slope values. The centers for an 8-bit ADC are shown in Figure 4.1. The standard deviation for all basis functions are set to be equal to the separation of the function's centers on the grid. Also the error estimation was done up to 12^{th} order intermodulation and harmonic terms of each calibration signal.

4.1 Simulation Results

Figures 4.2 to 4.3 show uncompensated and compensated spectra for a simulated 8-bit ADC. The simulated ADC model had error dependent on output sample, input slope and previous sample. The ADC model was selected to mimic the characteristics of a flash converter response. The uncompensated response has dominant second order slope dependent error at the higher frequencies and the

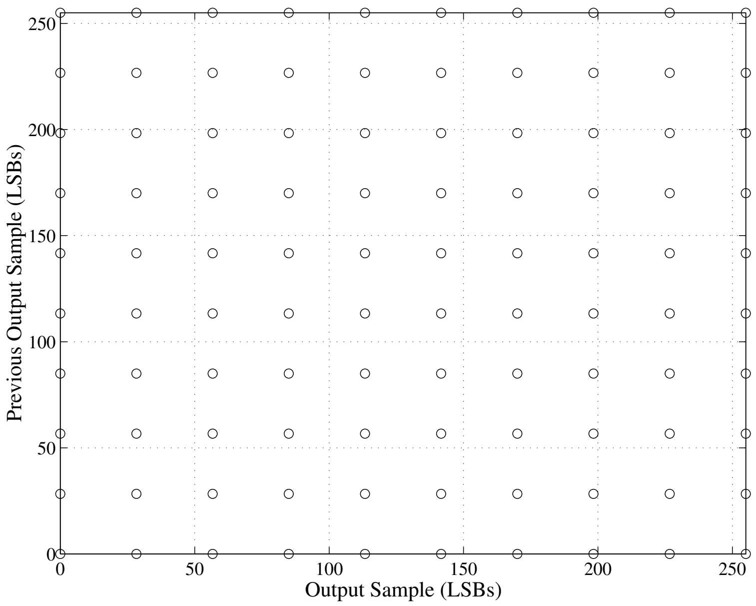

Figure 4.1: (c_{x_i}, c_{y_i}) basis function centers for $i = 1, \ldots, 60$.

previous and current sample errors are second and third order through the entire band. The graphs illustrate the ability of the multi-tone calibration to provide a sufficient error model to remove the harmonic distortion. Figure 4.5 is a plot of spurious free dynamic range (SFDR) measurements taken over the first Nyquist band of ADC. The SFDR results show the algorithm's ability to model all three types of error. The multi-tone calibration method has provided an error model that removes all error introduced in the simulated ADC.

4.2 Experimental Results

Figures 4.6 to 4.8 show uncompensated and compensated magnitude spectra for the experimental ADC. The 8-bit ADC was clocked at 204.8 MSPS. The basis functions and calibration signals for experimental testing were the same as those used for Section 4.1. The results show significant reduction of dominant harmonic distortion levels. The wideband calibration method is successfully modeling

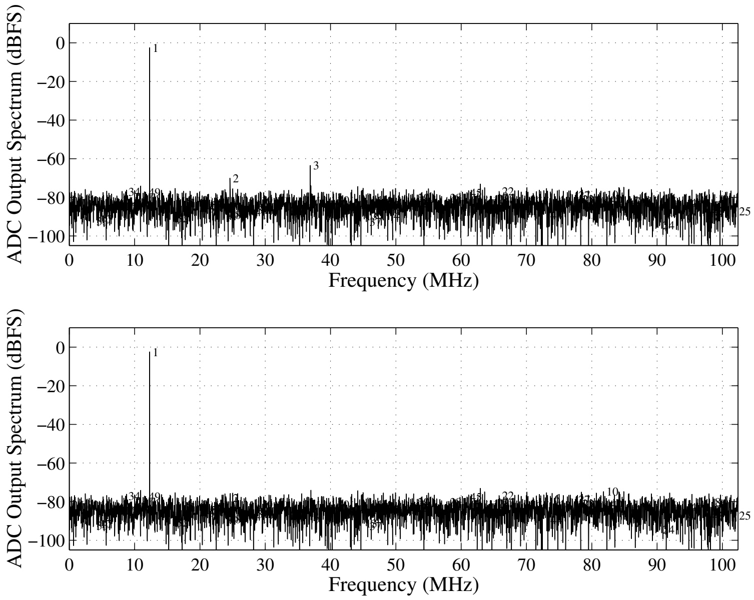

Figure 4.2: Uncompensated and compensated magnitude spectra, simulated results for a low frequency.

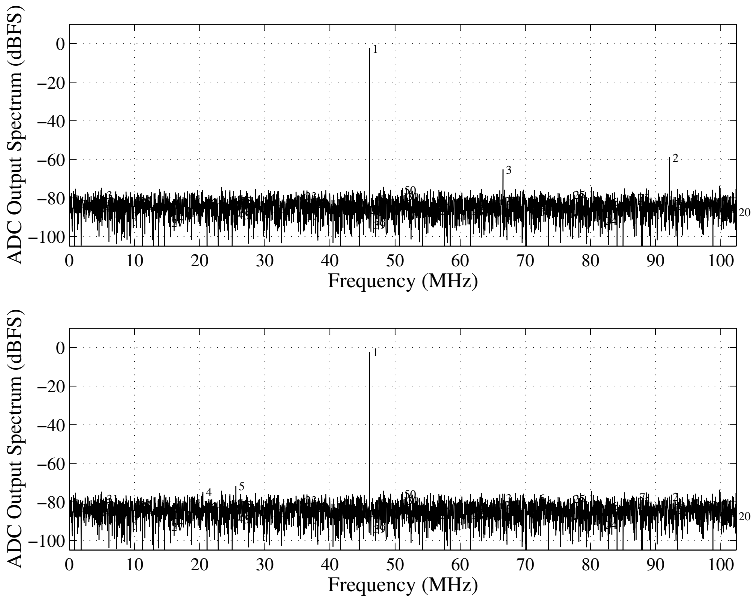

Figure 4.3: Uncompensated and compensated magnitude spectra, simulated results for a mid-Nyquist frequency.

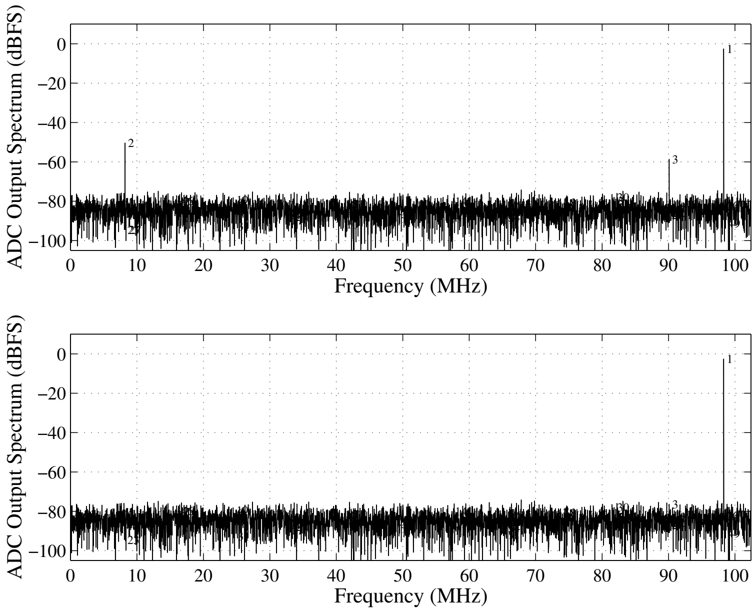

Figure 4.4: Uncompensated and compensated magnitude spectra, simulated results for a near-Nyquist frequency.

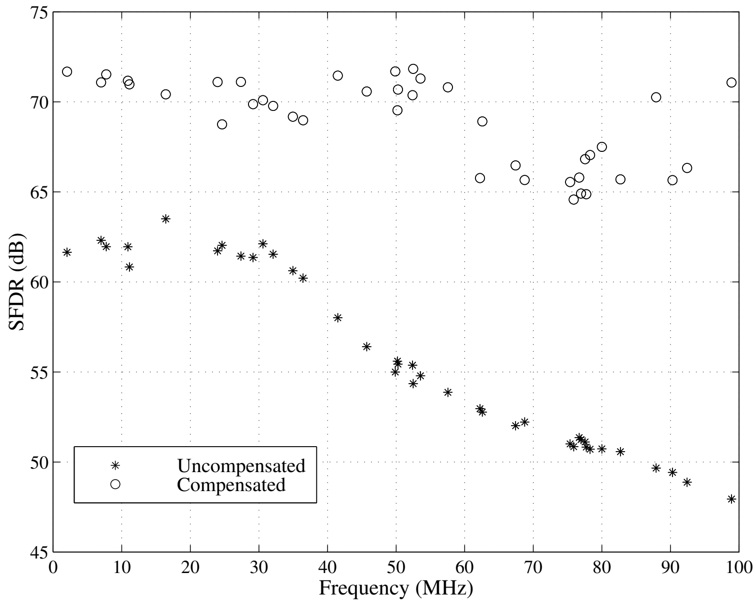

Figure 4.5: SFDR plot, simulated results.

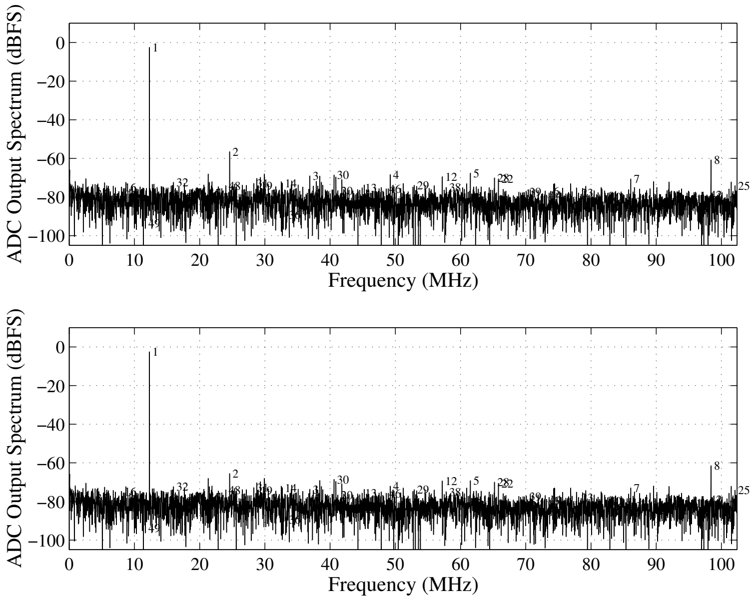

Figure 4.6: Uncompensated and compensated magnitude spectra, experimental results for a low frequency.

second and third order harmonic terms dependent on output sample, input slope and previous sample. Figure 4.9 shows the SFDR measurements across the first Nyquist band. The final multi-tone calibration method is providing a minimum of nearly 10 dB improvement in ADC resolution. The multi-tone calibration algorithm on the experimental ADC takes less than 5 minutes to run and matches or out performs other algorithms that take as much as 4 hours [2, 7]. Most importantly, the calibration is achieved using 25-50 times less data acquisition, the synthesizers can be replaced with 3 or 4 fixed frequency oscillators, and the filter bank is replaced with 2 low pass filters.

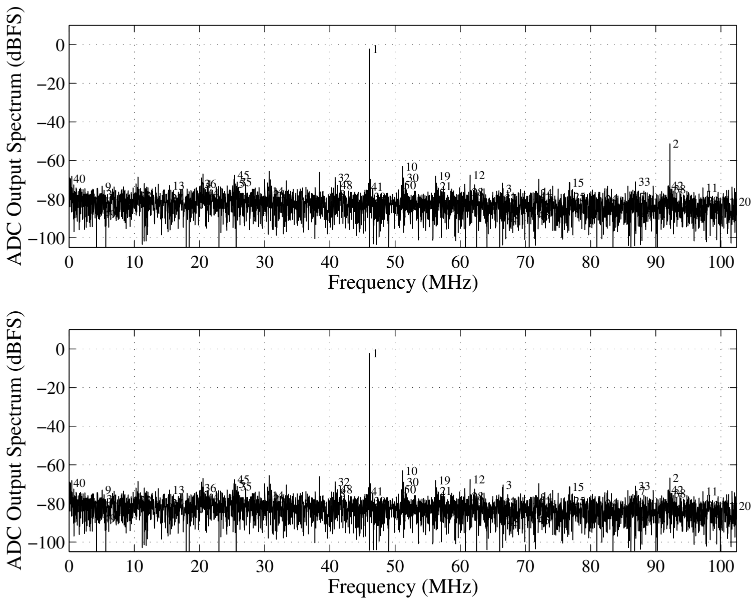

Figure 4.7: Uncompensated and compensated magnitude spectra, experimental results for a mid-Nyquist frequency.

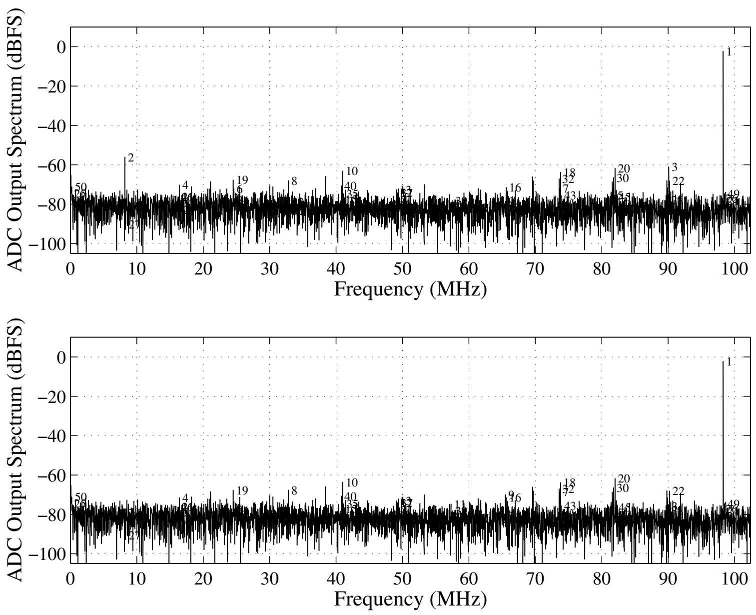

Figure 4.8: Uncompensated and compensated magnitude spectra, experimental results for a near-Nyquist frequency.

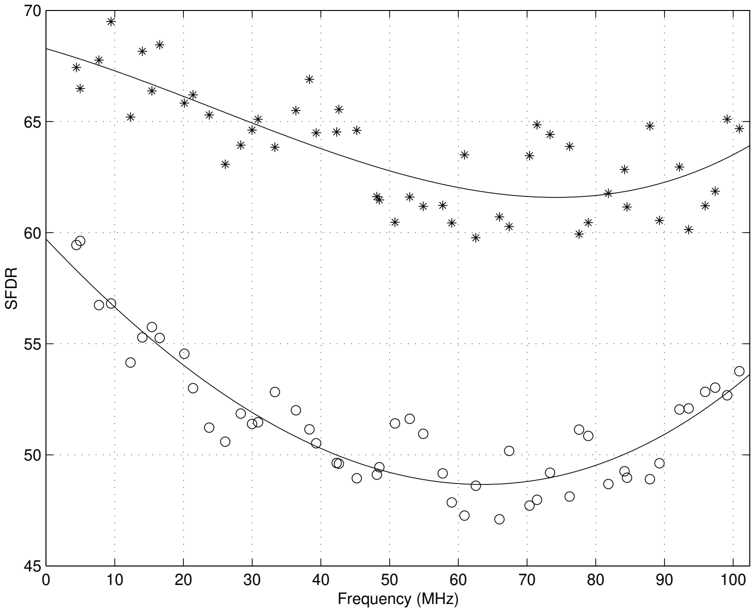

Figure 4.9: SFDR plot, experimental results.

CHAPTER 5

Conclusions

This thesis developed a new, faster calibration procedure for finding ADC error functions dependent on output sample, input slope and previous sample. Methods and criteria for selecting multi-tone calibration signals were also developed. The new algorithm was tested and shown to be a valid procedure through simulation testing on an ADC model containing sample, slope and previous sample errors only. The performance of the new method was then demonstrated by experimental testing on an actual ADC.

Two calibration signals were selected to provide sufficient data to determine an error model. The first signal, calibration signal 1, contained two tones of equal energy placed at high frequencies in the first Nyquist band. This signal excited the ADC at its full range of sample and slope combinations. The second two-tone calibration signal was determined to maximize the coverage of the possible combinations of sample and previous sample output data. The second signal, calibration signal 2, is limited to two tones which does not provide complete coverage of all possible data combinations. These calibration signals were sufficient for the scope of this thesis and provide a foundation for future specialized signals generated by digital-to-analog converters.

The two-tone calibration procedure was initially developed, in Chapter 2, to find error estimates dependent on sample and slope. The error functions were given a basis function representation where the functions were dependent upon sample and slope only. The estimate of the basis function coefficients, $\hat{\alpha}$, were found using a least-squares approach. Calibration signal 1 was the only signal used for the initial calibration attempts. Testing of the algorithm on a simulated ADC containing only sample and slope error, provided excellent results indicating that the one signal wideband calibration method was valid. Experimental results were not as successful and suggested that there might be additional sources of harmonic error in the ADC.

The two-tone calibration procedure was extended in Chapter 3 to include error dependent on the previous sample by using an additional calibration signal. The basis function approach added basis functions dependent upon sample and previous sample. This thesis assumed that the first set of basis functions and the new set were uncoupled. The estimate of the basis function coefficients was again found using a least-squares approach. Simulation results for an ADC model having error dependence on sample, slope, and previous sample, showed the effectiveness of the new algorithm to estimate errors of multiple sources with only two calibration signals. Experimental results show nearly 10 dB broadband improvement for the real ADC. The calibration signals and procedure estimated a substantial portion of the error in the real ADC.

The results of the multi-tone calibration methods presented in this thesis exceed those presented in previous work both in terms of performance and speed. The compensation results from the multi-tone method show 10 dB improvement in SFDR across the first Nyquist band. This result meets and exceeds other compensation results. The multi-tone method has reduced the number of calibration signals from 50-100 to 2. The reduction in number of calibration signals has eliminated the need for switchable filter banks and a wideband signal generator. The new method can utilize fixed frequency generators or digital-to-analog converter calibration signal generation. Most important the multi-tone calibration procedure is at least 20 times faster than any existing technique.

REFERENCES

[1] D. Asta and F.H. Irons. Dynamic error compensation of analog-to-digital converters. *The Lincoln Laboratory Journal*, 2:161–182, 1989.

[2] G.A. Friel, D.M. Hummels, and F.H. Irons. Simultaneous compensation of previous sample and slope dependent errors in analog to digital converters. In *3rd Intl. Conf. on Advanced A/D and D/A Conversion Techniques and Applications*, Glasgow, July 1999.

[3] D.M. Hummels, F.H. Irons, R. Cook, and I. Papantonopoulos. Characterization of ADCs using a non-iterative procedure. In *Proceedings of IEEE International Symp. on Circuits and Systems*, London, May 1994.

[4] F.H. Irons, D.M. Hummels, and S.P. Kennedy. Characterization of ADCs using a non-iterative procedure. *IEEE Trans. Circuits and Systems*, 38:958–961, 1991.

[5] R. Jacobson. Multi-band digital to analog converter compensation. Master's thesis, University of Maine, Dept. of Electrical and Computer Eng., Orono, ME, August 1999.

[6] Richard O. Hill Jr. *Elementary Linear Algebra with Applications.* Harcourt Brace Jovanovich, San Diego, California, 1991.

[7] J. Larrabee. ADC compensation using a sinewave histogram method. Master's thesis, University of Maine, Dept. of Electrical and Computer Eng., Orono, ME, May 1997.

[8] Alan V. Oppenheim and Ronald W. Shafer. *Discrete-Time Signal Processing.* Prentice Hall, Upper Saddle River, New Jersey, 1999.

[9] I.N. Papantonopoulos. Error modeling for folding and interpolation analog to digital converters. Master's thesis, University of Maine, Dept. of Electrical and Computer Eng., Orono, ME, August 1995.

[10] N.W. Spencer. Compensation of state-of-the-art analog to digital converters. Technical report, Project Report AST-4, M.I.T. Lincoln Laboratory, Lexington, Massachussets, March 1988.

APPENDIX

Singular Value Decomposition Methods

In section 2.4.1, the error in the ADC is given a basis function representation. The approximation to the basis function coefficients is determined in a least-squares manner. The result as presented in section 2.4.1 involves solving the system of equations

$$(B_T)^T(B_T)\hat{\vec{\alpha}} = (B_T)^T(\vec{x_T}) \tag{1}$$

Calculation of the inverse of the Gram matrix $(B_T)^T(B_T)$ in (.1) causes instabilities in the final solution of $\hat{\vec{\alpha}}$. If the matrix is singular the inverse does not exist. If the matrix has small sigular values, $\hat{\alpha}$ will do a good job eliminating the M harmonic error terms gathered from the calibration signal. However, other additional harmonics will be introduced into the solution. To stabilize the solution, a singular value decomposition method will be used.

A singular value decomposition of B_T produces three matrices, U, S and V [6].

$$B_T = USV^T \tag{2}$$

Where U is a matrix with columns given by the left singular vectors of B_T, $\vec{u}_k$. S is a diagonal matrix with diagonal elements which are the "singular values" of B_T, σ_j. V is a matrix with rows given by the right singular vectors of B_T, $\vec{v}_j$.

$$U = \begin{bmatrix} \vec{u}_0 & \vec{u}_1 & \vec{u}_2 & \dots & \vec{u}_{M-1} \end{bmatrix}$$

$$S = \begin{bmatrix} \sigma_0 & 0 & 0 & \dots & 0 \\ 0 & \sigma_1 & 0 & \dots & 0 \\ 0 & 0 & \sigma_2 & \dots & 0 \\ \vdots & & & \ddots & \\ 0 & 0 & 0 & \dots & \sigma_{M-1} \end{bmatrix} \tag{3}$$

$$\sigma_0 \geq \sigma_1 \geq \dots \geq \sigma_{M-2} \geq \sigma_{M-1} > 0$$

$$V = \begin{bmatrix} \vec{v}_0^T \\ \vec{v}_1^T \\ \vdots \\ \vec{v}_{M-1}^T \end{bmatrix}$$

The matrices U and V have the following identity properties.

$$U^T U = I$$
$$V^T V = I$$

Expanding (.2), B_T can be rewritten in a vector notation.

$$B_T = \sum_{i=0}^{M-1} \sigma_i \vec{u}_i \vec{v}_i^{\,T} \tag{4}$$

If the Gram matrix is nonsingular, then the singular values σ_i will be strictly positive. In this case, (.1) can be solved giving an expression for $\hat{\alpha}$.

$$\begin{aligned} \hat{\vec{\alpha}} &= ((B_T)^T(B_T))^{-1}(B_T)^T\vec{x}_T \\ &= (VS^TU^TUSV^T)^{-1}VS^TU^T\vec{x}_T \\ &= (VS^2V^T)^{-1}VS^TU^T\vec{x}_T \\ &= (VS^2V^T)^{-1}VS^TU^T\vec{x}_T \end{aligned}$$

$$
\begin{aligned}
&= VS^{-1}U^T\vec{x}_T \\
\hat{\vec{\alpha}} &= \sum_{i=0}^{M-1}\frac{1}{\sigma_i}\vec{v}_i\vec{u}_i^{\,T}\vec{x}_T
\end{aligned} \tag{5}
$$

Examining (.5), it is obvious that very small values of σ_i would cause instabilities in $\hat{\vec{\alpha}}$. If the Gram matrix is singular, then some of the singular values will be zero, and (.1) cannot be solved by matrix inversion. In this case the least squares solution is not unique, and many equivalent solutions for $\hat{\vec{\alpha}}$ may be found. The least squares solution which has the smallest length is given by truncating the summation in (.5) to include only the non-zero singular values [6]. If K is the number of zero singular values, the minimum length least square solution is given by (.6).

$$
\hat{\vec{\alpha}} = \sum_{i=0}^{M-K-1}\frac{1}{\sigma_i}\vec{v}_i\vec{u}_i^{\,T}\vec{x}_T \tag{6}
$$

In practice, because of noise in the measurements, the Gram matrix is rarely singular. However, in many cases singular values are small so that they are insignificant in the evaluation of (.4). In this case evaluating the inverse of the Gram matrix as in (.5) causes instabilities in the solution of $\hat{\vec{\alpha}}$. The resulting estimate minimizes the mean square error for the observed harmonics, but introduces significant distortion at frequencies not included in the calibration. An improved solution is obtained by setting some of these small singular values to zero, and evaluating (.6) instead of (.5). To implement this procedure, a criterion is developed for deciding which singular values to include in the summation.

In order to determine the smallest values of σ_i to include in the summation, we need to look at our error estimate formed from $\hat{\vec{\alpha}}$.

$$
\begin{aligned}
\hat{\vec{e}}_T &= B_T\hat{\vec{\alpha}} \\
&= \sum_{i=0}^{M-K-1}\frac{1}{\sigma_i}B_T\vec{v}_i\vec{u}_i^{\,T}\vec{x}_T
\end{aligned}
$$

$$= \sum_{i=0}^{M-K-1} \frac{1}{\sigma_i} \left[\sum_{j=0}^{M-K-1} \sigma_j \vec{u_j} \vec{v_j}^T \right] \vec{v_i} \vec{u_i}^T \vec{x}_T$$

$$\hat{\vec{e}_T} = \sum_{i=0}^{M-K-1} \vec{u_i} \vec{u_i}^T \vec{x}_T \tag{7}$$

$\hat{\vec{e}_T}$ is a vector which contains the real and imaginary components of various harmonics which will be predicted by the basis function expansion. To provide significant compensation of distortion caused by the ADC, values of $\hat{\vec{e}_T}$ must lie above the noise-floor of the converter's output spectrum. A reasonable criterion for dropping terms in the summation of (.6) is to drop as many small singular values as possible until the neglected terms in (.7) begin to exceed the noise-floor of the converter.

Let t be the value of the noise floor threshold which is determined from the statistics of the converter, and let w_k be defined as follows for values of $k = (0, 1, \ldots, M-1)$.

$$w_k = \max\left(\sum_{i=k}^{M-1} \vec{u_i} \vec{u_i}^T \vec{x}_T\right) \tag{8}$$

w_k represents the largest harmonic component from the dropped terms in (.7). As k decreases, more terms are included in (.8) and w_k grows, until it exceeds the noise threshold, t. Let K denote the index at which w_k exceeds t. Evaluation of (.6) then gives the desired coefficient estimates.

The selection of the noise threshold, t, must depend on the number of samples collected in the calibration buffer. In this thesis, t is determined using a statistical description of the FFT values stored in $\vec{x}_T$. The value of t is selected such that for an ideal dithered ADC, the noise floor for the FFT of an N-point buffer will remain below t with a fixed probability, p. Assuming an ideal quantizer, each dithered output sample will have zero mean and variance of $\frac{\delta^2}{6}$ where δ is the quantization interval [8]. For this thesis, sample values are measured in LSBs, giving $\delta = 1$. The complex values provided by the FFT of the sequence can be shown to have variance $\frac{\delta^2}{6}N$, where N is length of the FFT. Assuming that this error power is equally distributed between the real and imaginary parts of the FFT output, the variance in any given component of $\vec{x}_T$ is $\frac{1}{2}(\frac{\delta^2}{6})N = (\frac{\delta^2}{12})N = \frac{N}{12}$. If N is large, the noise in $\vec{x}_T$ will be normally distributed, with zero mean and variance $\frac{N}{12}$ denoted $N(0, \frac{N}{12})$.

The desired threshold needs to be set above the quantization noise floor in the output spectum. Let p_o equal the probability a sample from $\vec{x}_T$ is less than t.

$$p_o = P\{|N(0, \frac{N_s}{12})| < t\} \tag{9}$$

For a length N FFT, there are $2N$ output values (N complex outputs). The probability that all samples are less than t would be

$$p = p_o^{2N} \tag{10}$$

Now by selecting p, p_o can be found. p_o can then be used to find the threshold value, t, using the error function $\mathrm{erf}(x)$:

$$\mathrm{erf}(x) \triangleq \frac{2}{\sqrt{\pi}} \int_0^x e^{\lambda^2} d\lambda \tag{11}$$

Using (.11) to evaluate (.9) gives the interrelationship between p_o and t.

$$t = \sqrt{2}\sigma \mathrm{erf}^{-1}(p_0) \tag{12}$$

The value of p is determined through experimentation and then set. For purposes of this thesis p was selected to be 0.95. The choice of p becomes less significant as the number of samples increases. For an $N = 8192$ sample calibration buffer (.10) gives a value of $p_0 = 0.99999687$. Equation (.12) gives the required threshold, t. To use the singular value decomposition, w_k from (.8) is evaluated for k $= (0, 1, \ldots, M-1)$. K is selected as the index at which w_k exceeds t. The final estimated coefficients are determined from (.6).

Biography of the Author

Gina Kelso was born in Coos Bay, Oregon on December 31, 1974. She moved with her family to Clifton, Maine in December of 1979. She received her high school education from Brewer High School in Brewer, Maine in 1993.

She entered the University of Maine in 1993 and in 1995 she was selected to be the sixth Castle student. She obtained her Bachelor of Science degree in Electrical Engineering in 1997.

In May 1997, she is enrolled for graduate study in Electrical Engineering at the University of Maine and served as a Research Assistant. Her current research interests include communications and signal processing. She is a member of IEEE and Eta Kappa Nu, and her interests include travel and music.

She is a candidate for the Master of Science degree in Electrical Engineering from the University of Maine in August 1999.